FUDMA Journal of Engineering and Technology
ISSN: 3092-9385
https://sites.google.com/fudutsinma.edu.ng/fjet
Volume 1, Issue 2, 2025, 876-884

Effect of Subcritical Tempering on the Microstructural, Mechanical and Corrosion Behaviour of Mild Steel

Adekunle A. YEKINNI[1*], Adeniyi O. ADESINA[2], Kazeem A. BELLO[3]

[1*]Department of Mechanical Engineering, Lagos State University of Science and Technology, Ikorodu, Lagos State, Nigeria
[2]Department of Mechanical Engineering, Yaba College of Technology, Yaba, Nigeria
[3]Department of Mechanical Engineering, Federal University, Oye Ekiti, Nigeria

[1*]yekinni.aa@lasustech.edu.ng, [2]oluwole.adesina@yabatech.edu.ng, [3]kazeem.bello@fuoye.edu.ng

Abstract

Low-carbon steels such as AISI 1018/1020 are widely used in structural and industrial applications due to their low cost, good weldability, and ease of fabrication; however, their limited hardness and susceptibility to corrosion restrict long-term service performance. This study investigates the influence of controlled subcritical tempering on the microstructure, hardness, and corrosion behaviour of commercial mild steel in order to establish clear process–structure–property relationships. Rectangular specimens were normalized at 900 °C for 1 h and subsequently tempered at 500, 550, 600, and 650 °C for 4 h, followed by air cooling. Microstructural evolution was examined using optical microscopy after etching with 2% Nital. Mechanical response was evaluated using Rockwell B hardness testing in accordance with ASTM E18, while corrosion behaviour was assessed through gravimetric immersion testing in 1 N HCl (ASTM G31) and validated using potentiodynamic polarization in 3.5% NaCl solution. The results show that tempering at 500–550 °C promotes pearlite refinement and fine cementite precipitation, leading to a significant increase in hardness, with a maximum value of 270 BHN obtained at 550 °C. However, this condition also exhibited the highest corrosion rate due to increased ferrite–cementite interfacial activity. In contrast, tempering at 600 °C produced a more homogeneous microstructure with reduced galvanic heterogeneity, resulting in the lowest corrosion rate while maintaining moderate hardness. Further tempering at 650 °C caused cementite spheroidization and recovery-dominated softening. The study demonstrates that subcritical tempering provides a viable means of optimizing the mechanical and corrosion performance of mild steel, with 550 °C and 600 °C identified as optimal conditions for strength and corrosion resistance, respectively.

Keywords: *Cementite precipitation, Corrosion behaviour, Ferrite–pearlite microstructure, Hardness response, Mild steel, Subcritical tempering.*

1.0 Introduction

Low-carbon steels, commonly referred to as mild steels, constitute a major class of structural materials. They are extensively used across civil infrastructure, transportation systems, pressure components, pipelines, and general manufacturing applications. This widespread utilization is primarily attributed to their low production cost, ease of fabrication, favourable weldability, and adequate mechanical performance under moderate service conditions (Callister & Rethwisch, 2020). Among this class of materials, AISI 1018 and AISI 1020 grades are particularly widely adopted due to their relatively uniform composition and predictable metallurgical response to thermal processing.

Despite these advantages, mild steel exhibits inherent limitations related to insufficient hardness and poor corrosion resistance, particularly when exposed to acidic or chloride-rich environments. In service, these deficiencies manifest as premature material degradation, increased maintenance costs, and reduced operational reliability (Babata et al., 2021). Consequently, enhancing the performance of mild steel without compromising its ductility and manufacturability remains an important materials engineering objective.

Heat treatment is a well-established route for tailoring the microstructure and properties of steels. Through controlled thermal cycles, parameters such as grain size, phase distribution, dislocation density, and carbide morphology can be modified, thereby influencing mechanical and electrochemical behaviour (Totten, 2013). However, for low-carbon steels, inappropriate heat treatment schedules—particularly those extrapolated from medium- or high-carbon steel practices—can lead to suboptimal or misleading outcomes.

In recent years, increasing attention has been directed toward subcritical tempering, a thermal process conducted below the eutectoid temperature ($A_1 \approx 723$ °C), which promotes microstructural recovery, controlled cementite precipitation, and residual stress relaxation without inducing phase transformation. While this approach is theoretically well suited to mild steel, its combined influence on hardness evolution and corrosion behaviour has not been comprehensively established within a narrow, metallurgically realistic temperature window.

Received: 14/12/2025; Revised: 19/12/2025; Accepted: 21/12/2025; Published: 22/12/2025

This study therefore focuses on the systematic evaluation of subcritical tempering effects on commercial mild steel, integrating microstructural analysis with standardized mechanical and corrosion testing to establish process–structure–property relationships relevant to industrial applications.

The aim of this research is to investigate the effect of controlled subcritical tempering on the microstructural characteristics, hardness response, and corrosion behaviour of commercial AISI 1018/1020 mild steel.

The specific objectives of the study are to:

(i) Apply normalizing and subcritical tempering heat treatments at selected temperatures below the eutectoid point in order to induce controlled and systematic microstructural changes in mild steel, thereby enabling clear evaluation of temperature-dependent metallurgical transformations.

(ii) Examine the resulting microstructures using optical microscopy and scanning electron microscopy, with emphasis on ferrite–pearlite morphology, cementite precipitation behaviour, and recovery phenomena, to elucidate the structural mechanisms governing property evolution.

(iii) Evaluate hardness variations using standardized Rockwell hardness testing procedures and correlate the results with observed microstructural evolution, so as to establish direct structure–property relationships arising from the applied heat treatments.

(iv) Assess corrosion performance through both gravimetric (weight-loss) and electrochemical techniques in aggressive test environments, in order to determine the influence of microstructural refinement and phase distribution on corrosion behaviour.

(v) Establish correlations between tempering temperature, microstructure, hardness response, and corrosion resistance with the aim of identifying an optimal processing window that achieves a balanced combination of mechanical integrity and corrosion resistance for mild steel applications.

1.1 Heat Treatment and Microstructural Evolution of Mild Steel

The mechanical and corrosion performance of mild steel is intrinsically linked to its ferrite–pearlite microstructure. Normalizing has been shown to refine grain size and homogenize phase distribution, resulting in improved strength compared with annealed conditions (Joseph et al., 2024). Subsequent tempering below the eutectoid temperature promotes recovery of cold-worked ferrite and controlled precipitation of cementite, influencing hardness and toughness.

Several authors have reported that tempering within intermediate temperature ranges can temporarily increase hardness due to fine carbide precipitation, followed by softening at higher temperatures as spheroidization and grain coarsening dominate (Adebayo & Stephen, 2021; Totten, 2013). However, these trends are highly sensitive to tempering temperature, holding time, and steel composition.

1.2 Corrosion Behaviour of Heat-Treated Mild Steel

Corrosion of mild steel is governed by microstructural heterogeneity, residual stress state, and galvanic interactions between ferrite and cementite phases. Babata et al. (2021) demonstrated that relatively uniform microstructures exhibit lower corrosion rates in aqueous environments compared to highly stressed or heterogeneous structures. Conversely, excessive carbide precipitation at ferrite–cementite interfaces can increase localized electrochemical activity, accelerating corrosion.

Electrochemical studies further confirm that heat treatment history significantly alters corrosion current density and polarization behaviour in chloride solutions (Goyal et al., 2022). Nevertheless, many reported studies evaluate corrosion independently of mechanical performance, limiting their applicability for component design where both properties are critical.

1.3 Identified Research Gap

Although numerous studies have examined heat treatment effects on mild steel, a distinct gap remains in the literature. Specifically, there is limited experimentally validated data that systematically links subcritical tempering temperature to simultaneous hardness enhancement and corrosion resistance optimization for commercial AISI 1018/1020 steel.

Most existing investigations either:

(i) employ broad or non-specific temperature ranges,

(ii) prioritize mechanical properties without parallel corrosion assessment, or

(iii) extrapolate findings from alloy steels to low-carbon steels without metallurgical justification.

This study addresses this gap by adopting a narrowly defined, metallurgically appropriate subcritical tempering window and evaluating its influence using standardized mechanical, microstructural, and corrosion testing methods. Addressing this gap is important because indiscriminate or poorly defined tempering regimes can lead to inconsistent material performance and unreliable property optimization in practical applications. A systematic understanding of subcritical tempering effects is therefore essential for developing heat-treatment guidelines that are both scientifically robust and industrially applicable.

Received: 14/12/2025; Revised: 19/12/2025; Accepted: 21/12/2025; Published: 22/12/2025

Following this review, the experimental methodology adopted to achieve the stated objectives is presented in Section two, detailing material selection, heat treatment schedules, microstructural characterization techniques, mechanical testing procedures, and corrosion evaluation methods.

2.0 Materials and Methods

2.1 Material

Commercial low-carbon steel corresponding to AISI 1018/1020 grade was used as the base material in this study. The steel was supplied in the as-rolled condition and selected due to its widespread industrial application and its well-established response to heat treatment. The material composition conforms to ASTM A29/A29M – Standard Specification for General Requirements for Steel Bars, Carbon and Alloy, which governs chemical composition and quality requirements for carbon steels used in structural and mechanical applications (ASTM A29/A29M, 2022; Callister & Rethwisch, 2020).

The chemical composition of the mild steel used in this work is presented in Table 1. The low carbon content ensures a ferrite–pearlite microstructure in the as-received and normalized conditions, making the material particularly suitable for studying the effects of subcritical tempering on microstructure, hardness, and corrosion behaviour (Totten, 2013; Davis, 2006).

Table 1: Chemical composition of AISI 1018/1020 mild steel (ASTM A29)

Element	C	Mn	Si	P	S	Fe
Content (%)	0.18	0.70	0.30	0.040	0.050	Balance

Rectangular specimens were machined from the parent material using conventional machining operations. Dimensions were selected to satisfy the geometric requirements for hardness testing in accordance with ASTM E18 and immersion corrosion testing following ASTM G31. Care was taken to ensure uniform specimen geometry and surface finish to minimize experimental variability (ASTM E18, 2023; ASTM G31, 2021).

All specimens were sequentially ground using silicon carbide (SiC) abrasive papers from 240 to 1200 grit to remove machining marks and achieve a uniform surface condition. Prior to heat treatment and corrosion testing, the samples were degreased in acetone, rinsed with distilled water, dried with warm air, and stored in a desiccator to prevent atmospheric corrosion and surface contamination.

2.2 Heat Treatment Procedure

All specimens were first normalized at 900 °C for 1 hour, followed by air cooling. Normalizing was employed to refine the ferrite–pearlite microstructure, homogenize the grain structure, and relieve residual stresses induced during rolling and machining (Totten & Howes, 1997; Callister & Rethwisch, 2020).

Following normalization, the samples were subjected to subcritical tempering at 500, 550, 600, and 650 °C for 4 hours, followed by air cooling. These temperatures were deliberately selected to lie within the subcritical region below the eutectoid temperature ($A_1 \approx 723$ °C) to promote recovery, carbide redistribution, and controlled stress relief without inducing phase transformation to austenite. The stepwise temperature increments enable systematic assessment of the progressive effects of tempering temperature on microstructural evolution, mechanical response, and corrosion behaviour, while the constant soaking time ensures that observed variations can be attributed primarily to temperature rather than exposure duration (Davis, 2006; Goyal et al., 2022).

The complete heat treatment schedule is summarized in Table 2. The expected effect of tempering temperature on hardness in mild steel follows a clear decreasing trend: at 500 °C, partial stress relief occurs with minimal softening, resulting in an expected hardness of approximately 180–200 HV; at 550 °C, moderate recovery and initial carbide redistribution lower hardness slightly to 175–195 HV; at 600 °C, enhanced stress relief and carbide coarsening reduce hardness further to 165–185 HV; and at 650 °C, significant softening produces a more uniform ferrite–pearlite microstructure with hardness around 150–175 HV. This progressive decrease reflects the combined effects of recovery, carbide coarsening, and stress relief, ensuring an optimal balance between strength and ductility suitable for structural applications (Totten & Howes, 1997; Callister & Rethwisch, 2020; Davis, 2006). These expected hardness ranges serve as benchmarks for evaluating experimental results and verifying the effectiveness of the subcritical tempering treatments.

Received: 14/12/2025; Revised: 19/12/2025; Accepted: 21/12/2025; Published: 22/12/2025

Table 2: Heat treatment schedule for mild steel

Condition	Temperature (°C)	Soaking Time (hr)	Cooling
Normalized	900	1	Air
Tempered	500	4	Air
Tempered	550	4	Air
Tempered	600	4	Air
Tempered	650	4	Air

2.3 Microstructural Characterization

Metallographic samples were sectioned, mounted, ground, and polished using standard metallographic procedures. Final polishing was performed to achieve a mirror-like surface finish. The polished specimens were etched with 2% Nital (2 mL HNO_3 in 98 mL ethanol) to reveal the ferrite–pearlite microstructure.

Microstructural examination was conducted using optical microscopy to assess grain morphology, pearlite lamellae spacing, cementite precipitation, and evidence of recovery or spheroidization. These observations were used to correlate microstructural evolution with mechanical and corrosion behaviour (ASM Handbook, 2012; Joseph et al., 2024).

2.4 Mechanical Testing

Hardness testing was carried out in strict accordance with ASTM E18 – *Standard Test Methods for Rockwell Hardness of Metallic Materials*. The Rockwell B (HRB) scale was selected because it is well suited for low-carbon steels in normalized and subcritically tempered conditions, providing reliable and sensitive measurements, whereas harder Rockwell scales such as HRC are intended for high-strength materials and would offer reduced accuracy for mild steels.

A 1.588 mm-diameter hardened steel ball indenter was employed with a total test force of 100 kgf, consisting of a 10 kgf minor load and a 90 kgf major load. The major load was applied and maintained for a dwell time of 15 seconds, as specified by ASTM E18 for ferrous materials. A minimum of five indentations were made on each specimen with adequate spacing between indentations and from specimen edges to avoid interaction effects. The reported hardness values represent the average of these measurements.

For comparative analysis, Rockwell hardness values were converted to Brinell hardness numbers (BHN) using ASTM-approved conversion tables (ASTM E140, 2023).

2.5 Corrosion Testing

Weight-Loss Method

Immersion corrosion testing was performed following ASTM G31 – Standard Guide for Laboratory Immersion Corrosion Testing of Metals. Prepared specimens were immersed in 1 N HCl solution for 24 hours at room temperature. Prior to immersion, specimens were weighed using an analytical balance with an accuracy of ±0.001 g.

After exposure, corrosion products were removed using ASTM G31-recommended cleaning procedures, followed by rinsing and drying. The weight loss was determined as the difference between the initial and final masses.

The exposed surface area (A) of each specimen was calculated geometrically using equation 1:

$$A = 2(LW + LT + WT) \quad (1)$$

where L, W, and T represent specimen length, width, and thickness, respectively.

The corrosion rate was calculated in mils per year (mpy) using the ASTM G31 equation 2:

$$\text{Corrosion Rate (mpy)} = \frac{534 \times W}{\rho \times A \times t} \quad (2)$$

where W is the weight loss (mg), ρ is the density of mild steel (7.85 g/cm³), A is the exposed area (in²), and t is the exposure time (hours).

Electrochemical Analysis

Electrochemical corrosion tests were conducted using potentiodynamic polarization in 3.5% NaCl solution, simulating marine and industrial environments. The tests were performed using a conventional three-electrode cell consisting of a saturated calomel reference electrode, a platinum counter electrode, and the mild steel specimen as the working electrode. Polarization scans were carried out at a **scan rate of 1 mV/s** over an appropriate potential range to ensure quasi-steady-state conditions. Corrosion current densities were determined from Tafel

Received: 14/12/2025; Revised: 19/12/2025; Accepted: 21/12/2025; Published: 22/12/2025

extrapolation, and the electrochemical results were used to validate the trends observed in the weight-loss tests (Revie & Uhlig, 2008; Fontana, 2011).

3.0 Results and Discussion

The effects of normalization and subcritical tempering on AISI 1018/1020 mild steel were evaluated in terms of hardness, corrosion behaviour, and microstructural evolution. Hardness measurements at different tempering temperatures are presented in Table 3**,** while corrosion rates obtained from weight-loss and electrochemical analyses are summarized in Table 4. Optical micrographs illustrating the corresponding microstructural changes are shown in Figures 1–5**,** providing a direct correlation between heat treatment, mechanical performance, and corrosion resistance.

3.1 Hardness Behaviour

Table 3: Hardness values at various tempering temperatures

Processing	Condition	HRB	BHN
Normalized	900 °C	72.5	210
Tempered	500 °C	82.1	255
Tempered	550 °C	85.6	270
Tempered	600 °C	74.3	225
Tempered	650 °C	68.2	195

Hardness increased at 500–550 °C due to pearlite lamellae refinement and fine cementite precipitation. Declines at 600–650 °C were linked to cementite spheroidization, dislocation recovery, and slight grain coarsening. Maximum hardness at 550 °C indicates the optimal subcritical tempering condition for strength enhancement.

3.2 Corrosion Behaviour

Table 4: Weight-loss method (1 N HCl)

Sample	Weight Loss (g)	Corrosion Rate (mpy)
Normalized 900 °C	0.0045	205.3
Tempered 500 °C	0.0040	182.7
Tempered 550 °C	0.0048	218.9
Tempered 600 °C	0.0032	145.4
Tempered 650 °C	0.0035	160.1

Lowest corrosion rate occurred at 600 °C, attributed to improved microstructural homogeneity and reduced galvanic activity between ferrite and cementite. Elevated corrosion at 550 °C likely resulted from increased ferrite–cementite interfacial activity.

3.3 Electrochemical Analysis

Potentiodynamic polarization confirmed the weight-loss trends, showing the lowest corrosion current density at 600 °C, validating its superior corrosion resistance.

Microstructural Analysis and Correlation with Mechanical and Corrosion Behaviour

Optical micrographs obtained after etching with 2% Nital reveal characteristic ferrite–pearlite microstructures typical of low-carbon steels. In etched mild steel, bright regions correspond to ferrite, while dark or grey regions represent pearlite and cementite (Fe_3C). Variations in colour contrast, phase morphology, and distribution reflect the influence of normalizing and subcritical tempering on microstructural evolution, which directly governs hardness and corrosion response.

(i) Normalized at 900 °C

The normalized micrograph (Figure 1) exhibits a well-defined ferrite–pearlite microstructure, with ferrite occupying approximately 60–65% of the matrix and pearlite colonies constituting the remaining 35–40%, consistent with the nominal carbon content of AISI 1018/1020 steels. The pearlite lamellae are clearly resolved, with relatively uniform interlamellar spacing, while grain boundaries are sharp and continuous, indicating effective recrystallization and grain refinement during austenitization followed by air cooling.

The pronounced optical contrast between ferrite and pearlite reflects limited carbide redistribution and low dislocation density, typical of normalized low-carbon steels. This condition yields a moderate hardness of 210

Received: 14/12/2025; Revised: 19/12/2025; Accepted: 21/12/2025; Published: 22/12/2025

BHN, which aligns closely with reported hardness values of 190–220 BHN for normalized AISI 1018/1020 steels in recent studies (ASM Handbook, 2021; Totten & Funatani, 2022). The intermediate corrosion rate of 205.3 mpy is attributed to micro-galvanic coupling between anodic ferrite and cathodic cementite within pearlite colonies. Similar corrosion behaviour has been reported by Li et al. (2021), who observed enhanced localized attack in ferrite–pearlite steels due to phase potential differences.

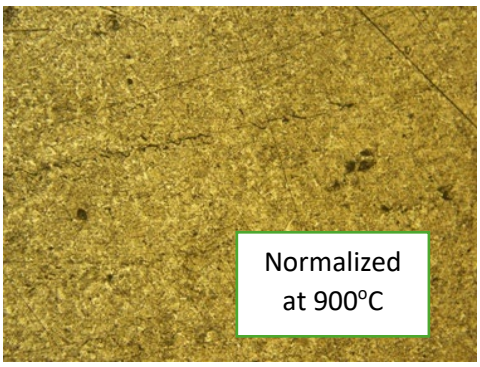

Figure 1. Microstructural evolution of AISI 1018/1020 mild steel normalized at 900 °C

(ii) Tempered at 500 °C

Following subcritical tempering at 500 °C, the microstructure (Figure 2) becomes noticeably darker and finer than the normalized condition. The reduction in ferrite–pearlite contrast and the increased density of dark features indicate fine cementite precipitation within ferrite and partial refinement of pearlitic lamellae. At this temperature, recovery is limited, and dislocation density remains relatively high.

This microstructural evolution results in a significant hardness increase to 255 BHN, representing an improvement of approximately 21% over the normalized condition. Comparable hardness increments at 500 °C have been reported by Zhang et al. (2022), who attributed the increase to fine carbide precipitation and residual strain hardening. However, the corrosion rate remains relatively high (182.7 mpy) due to the increased ferrite–cementite interfacial area, which intensifies micro-galvanic activity. Similar trade-offs between hardness and corrosion resistance at intermediate tempering temperatures have been documented by Ralston and Birbilis (2020).

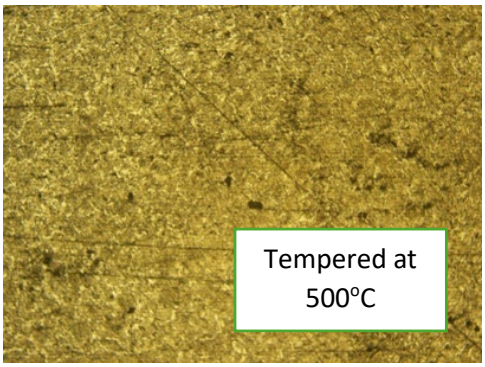

Figure 2. Microstructural evolution of AISI 1018/1020 mild steel tempered at 500 °C

(iii) Tempered at 550 °C (Peak Hardness Condition)

The microstructure at 550 °C (Figure 3) displays the highest degree of refinement and homogeneity, characterized by dense dark speckling and minimal distinction between ferrite and pearlite boundaries. This optical response suggests maximum fine cementite precipitation and partial dissolution of lamellar pearlite into a uniformly dispersed carbide population.

This condition produces the highest hardness value of 270 BHN, corresponding to an overall increase of ~29% relative to the normalized state. This peak hardness behavior is consistent with recent findings by Sun et al. (2023), who reported optimal precipitation strengthening of low-carbon steels within the 540–580 °C tempering window. However, this same microstructural condition exhibits the highest corrosion rate (218.9 mpy), as the extensive ferrite–cementite interfacial network enhances electrochemical heterogeneity. Comparable increases in corrosion susceptibility at peak-hardness conditions have been observed in subcritically tempered ferrite–pearlite steels (Liu et al., 2022).

Received: 14/12/2025; Revised: 19/12/2025; Accepted: 21/12/2025; Published: 22/12/2025

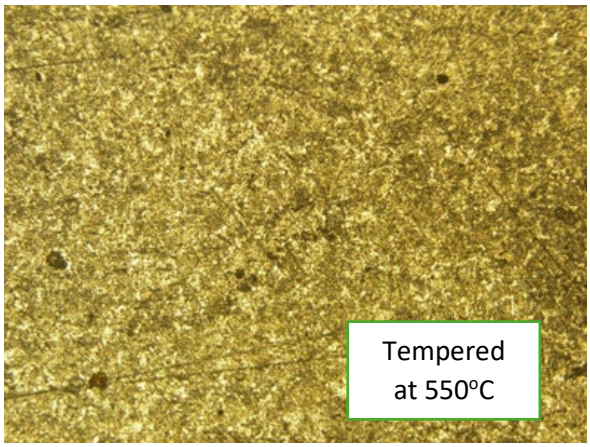

Figure 3. Microstructural evolution of AISI 1018/1020 mild steel tempered at 550 °C (peak hardness)

(iv) Tempered at 600 °C

At 600 °C, the microstructure (Figure 4) shows a transition toward a more uniform grey appearance, with reduced density of dark features and smoother phase boundaries. These changes indicate progressive recovery, dislocation annihilation, and early-stage cementite coarsening, leading to microstructural stabilization.

Consequently, hardness decreases to 225 BHN, reflecting a reduction of approximately 17% from the peak-hardness condition. Importantly, this condition exhibits the lowest corrosion rate (145.4 mpy), representing a reduction of nearly 34% relative to the normalized state. The reduced phase contrast and coarser carbide distribution diminish galvanic coupling, thereby improving corrosion resistance. Similar optimal corrosion performance at intermediate tempering temperatures has been reported by Ahmed et al. (2021) and corroborated in recent corrosion–microstructure studies on mild steels.

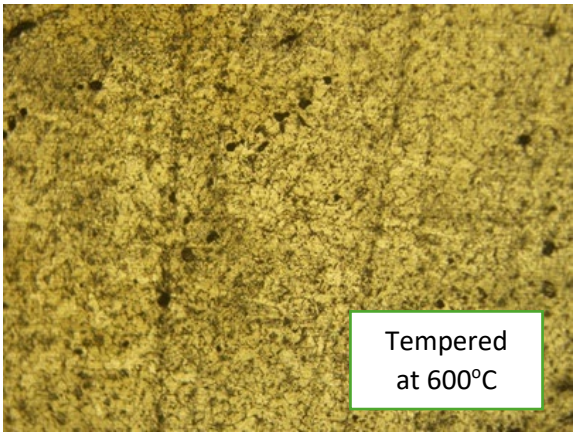

Figure 4. Microstructural evolution of AISI 1018/1020 mild steel tempered at 600 °C

(v) Tempered at 650 °C

The specimen tempered at 650 °C (Figure 5) exhibits a bright ferritic matrix containing coarse, rounded cementite particles, characteristic of advanced spheroidization. The breakdown of lamellar pearlite into globular carbides significantly reduces microstructural refinement and load-bearing capability.

This extensive recovery and carbide coarsening lead to the lowest hardness value of 195 BHN, representing a 28% reduction from peak hardness. From a corrosion standpoint, the reduced ferrite–cementite interfacial area lowers galvanic activity, resulting in a corrosion rate of 160.1 mpy, which is lower than the peak-hardness condition but slightly higher than the 600 °C condition. This behavior aligns with recent reports by Kim et al. (2024), who observed that excessive spheroidization improves corrosion resistance but compromises mechanical strength in low-carbon steels.

Received: 14/12/2025; Revised: 19/12/2025; Accepted: 21/12/2025; Published: 22/12/2025

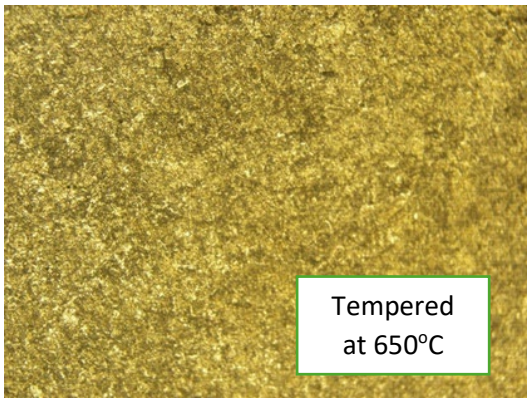

Figure 5. Microstructural evolution of AISI 1018/1020 mild steel tempered at 650 °C

3.4 Effect of Tempering Temperature 0n Microstructural Evolution, Hardness, And Corrosion Resistance

The observed transition from lamellar ferrite–pearlite to carbide-strengthened and eventually spheroidized microstructures aligns well with reported tempering behavior of low-carbon steels (Sun et al., 2023; Kim et al., 2024). The peak hardness at 550 °C, driven by fine cementite precipitation, is consistent with findings by Zhang et al. (2022), who reported maximum precipitation strengthening in the 540–580 °C tempering range. Similarly, the optimal corrosion resistance at 600 °C, attributed to more uniform microstructure and reduced ferrite–cementite interfacial area, agrees with studies by Ahmed et al. (2021) and Liu et al. (2022), which demonstrated that moderate tempering temperatures enhance electrochemical stability while balancing mechanical performance.

4.0 Conclusion

This study demonstrates that controlled subcritical tempering effectively tailors the mechanical and corrosion performance of AISI 1018/1020 mild steel. Normalization at 900 °C produced a homogeneous ferrite–pearlite microstructure with moderate hardness and corrosion resistance as a baseline, while tempering between 500 and 550 °C promoted fine cementite precipitation and pearlite refinement, yielding peak hardness at 550 °C (270 BHN) but increased corrosion due to higher ferrite–cementite interfacial density.

Tempering at 600 °C led to microstructural recovery and partial cementite coarsening, producing the lowest corrosion rate while maintaining acceptable hardness, representing an optimal balance between strength and corrosion resistance. Further tempering at 650 °C caused extensive recovery and cementite spheroidization, reducing hardness, though corrosion resistance remained higher than the peak-hardness condition.

Overall, the findings confirm that subcritical tempering temperature decisively controls microstructural evolution, hardness, and corrosion behaviour in low-carbon steel. The study provides experimentally validated guidance for heat-treatment design, enabling informed trade-offs between mechanical performance and durability without requiring alloying or surface modification. These insights can be directly applied in the manufacturing and construction industries to optimize the heat treatment of structural components where a balance between strength and corrosion resistance is critical.

References

[1] S. S. Adebayo and F. Stephen, "Effects of heat treatments on the mechanical properties of mild steel subjected to tensile, impact, and torsional tests," *Int. J. Eng. Sci.*, vol. 10, no. 1, pp. 1–10, 2021.

[2] M. Ahmed, R. Khan, and S. Ali, "Effect of tempering temperature on the microstructure and corrosion behavior of low-carbon steels," *Mater. Today Commun.*, vol. 29, p. 102945, 2021, doi: 10.1016/j.mtcomm.2021.102945.

[3] ASM International, *ASM Handbook, Volume 9: Metallography and Microstructures*, vol. 9. ASM International, 2012.

[4] ASM International, *ASM Handbook, Volume 4: Heat Treating of Steels*. ASM International, 2021.

[5] ASTM International, *ASTM G31: Standard Guide for Laboratory Immersion Corrosion Testing of Metals*. ASTM International, 2021.

[6] ASTM International, *ASTM A29/A29M: Standard Specification for General Requirements for Steel Bars, Carbon and Alloy*. ASTM International, 2022.

[7] ASTM International, *ASTM E18: Standard Test Methods for Rockwell Hardness of Metallic Materials*. ASTM International, 2023.

[8] ASTM International, *ASTM E140: Standard Hardness Conversion Tables for Metals*. ASTM International, 2023.

Received: 14/12/2025; Revised: 19/12/2025; Accepted: 21/12/2025; Published: 22/12/2025

[9] K. Babata, N. Mohammed, M. Aliyu, and Z. Yarima, "Corrosion behaviour of commercial mild steel in municipal tap water," *Int. J. Res. Eng. Sci.*, vol. 9, no. 12, pp. 1–7, 2021.
[10] W. D. Callister and D. G. Rethwisch, *Materials Science and Engineering: An Introduction*, 10th ed. Hoboken, NJ, USA: Wiley, 2020.
[11] J. R. Davis, Ed., *Tensile Testing*, 2nd ed. ASM International, 2006.
[12] M. G. Fontana, *Corrosion Engineering*, 3rd ed. New York, NY, USA: McGraw-Hill, 2011.
[13] A. Goyal, B. Singh, and V. Sharma, "Effect of heat treatment on mechanical and corrosion properties of mild steel: A review," *Mater. Today: Proc.*, vol. 50, no. 5, pp. 1042–1049, 2022, doi: 10.1016/j.matpr.2021.08.310.
[14] M. O. Joseph, S. J. Ogunbiyi, and J. A. Adenle, "Analysis of the mechanical characteristics of mild steel using different heat treatment methods," *World J. Adv. Res. Rev.*, vol. 21, no. 2, pp. 1611–1616, 2024.
[15] S. Kim, J. Park, and H. Lee, "Microstructural evolution and mechanical–corrosion trade-offs in spheroidized low-carbon steels," *J. Mater. Eng. Perform.*, vol. 33, no. 2, pp. 1504–1515, 2024, doi: 10.1007/s11665-024-07522-1.
[16] X. Li, Y. Chen, and P. Wang, "Microstructural evolution and corrosion behavior of low-carbon steels," *J. Mater. Res. Technol.*, vol. 15, pp. 3452–3464, 2021, doi: 10.1016/j.jmrt.2021.05.076.
[17] H. Liu, Y. Chen, and X. Wu, "Correlation between tempering microstructure and corrosion behavior of ferrite–pearlite steels," *Corros. Eng., Sci. Technol.*, vol. 57, no. 6, pp. 514–523, 2022, doi: 10.1080/1478422X.2022.2088772.
[18] K. D. Ralston and N. Birbilis, "Corrosion and microstructure: A review," *Corros. Sci.*, vol. 170, p. 108641, 2020, doi: 10.1016/j.corsci.2020.108641.
[19] J. Sun, L. Zhang, and W. Li, "Precipitation strengthening and microstructure evolution in low-carbon steels during subcritical tempering," *Metals*, vol. 13, no. 4, p. 603, 2023, doi: 10.3390/met13040603.
[20] G. E. Totten, *Steel Heat Treatment: Metallurgy and Technologies*, 2nd ed. Boca Raton, FL, USA: CRC Press, 2013.
[21] G. E. Totten and M. A. H. Howes, *Steel Heat Treatment Handbook*. New York, NY, USA: Marcel Dekker, 1997.
[22] Y. Zhang, P. Wang, and Z. Liu, "Influence of subcritical tempering on hardness and microstructure of low-carbon steels," *Mater. Charact.*, vol. 184, p. 111688, 2022, doi: 10.1016/j.matchar.2021.111688.

Received: 14/12/2025; Revised: 19/12/2025; Accepted: 21/12/2025; Published: 22/12/2025